Published in final edited form as:
J Microsc. 2010 November ; 240(2): 155–163. doi:10.1111/j.1365-2818.2010.03389.x.

Automated focusing in bright-field microscopy for tuberculosis detection

O.A. OSIBOTE, **R. DENDERE**, **S. KRISHNAN**, and **T.S. DOUGLAS**
MRC/UCT Medical Imaging Research Unit, Department of Human Biology, University of Cape Town, South Africa

Summary

Automated microscopy to detect *Mycobacterium tuberculosis* in sputum smear slides would enable laboratories in countries with a high tuberculosis burden to cope efficiently with large numbers of smears. Focusing is a core component of automated microscopy, and successful autofocusing depends on selection of an appropriate focus algorithm for a specific task. We examined autofocusing algorithms for bright-field microscopy of Ziehl–Neelsen stained sputum smears. Six focus measures, defined in the spatial domain, were examined with respect to accuracy, execution time, range, full width at half maximum of the peak and the presence of local maxima. Curve fitting around an estimate of the focal plane was found to produce good results and is therefore an acceptable strategy to reduce the number of images captured for focusing and the processing time. Vollath's F_4 measure performed best for full z-stacks, with a mean difference of 0.27 μm between manually and automatically determined focal positions, whereas it is jointly ranked best with the Brenner gradient for curve fitting.

Keywords

Autofocusing; automated microscopy; focus measure; tuberculosis; Ziehl-Neelsen

Introduction

Timely and accurate diagnosis of tuberculosis (TB) is needed to improve treatment, reduce transmission and control the development of drug resistance. Although microscopy remains the cornerstone of TB screening in low- and middle-income countries, such screening is labour intensive and has variable sensitivity (Steingart *et al.*, 2006); a technician is expected to spend at least 15 min per slide and to examine at least 100 fields in each slide, and can therefore examine a limited number of slides in a day (Sadaphal *et al.*, 2008). Automation of microscopy for TB screening aims to speed up the screening process, to improve its sensitivity and to reduce its reliance on technicians.

Steps in automated microscopy include autofocusing, image capture, image segmentation and object classification. Algorithms for segmentation and classification of *Mycobacterium tuberculosis* in sputum smear images have been published for Ziehl–Neelsen (ZN) and for auramine stained smears (Veropoulos *et al.*, 1999; Forero *et al.*, 2006; Sadaphal *et al.*, 2008; Khutlang *et al.*, 2010, in press). Autofocusing is a critical step in automated microscopy, as

Correspondence to: Tania S. Douglas, Department of Human Biology, Faculty of Health Sciences, University of Cape Town, Observatory 7935, South Africa. Tel: +27-21-4066541; fax: +27-21-4487226; tania@ieee.org.

subsequent image analysis steps depend on it, and better-focused images can be expected to yield better segmentation and classification results.

A well-focused image has the best average focus over an entire field of view, even though objects often reside at multiple foci in thick sample slides. Several autofocusing methods have been proposed and compared for different biological and biomedical applications but the selection of an appropriate method for a specific sample and application remains task-dependent (Sun *et al.*, 2004). Some methods have been reported to be optimal for fluorescence images (Vollath, 1988; Santos *et al.*, 1997) but less suitable for bright-field microscopy. Pech-Pacheco *et al.* (2000) compared focus methods for diatom detection and identification in bright-field microscopy, whereas Liu *et al.* (2007) investigated focusing for pap smear and blood smear microscopy. Sun *et al.* (2004) compared autofocusing algorithms for bright-field, phase contrast and differential interference contrast microscopy. Forero *et al.* (2004) used an autofocusing algorithm in fluorescence TB microscopy. To the authors' knowledge, autofocusing algorithms have not been compared towards the selection of a suitable method for autofocusing in bright-field TB microscopy.

Typically, the autofocus algorithm establishes a correspondence between the level of the microscope stage with respect to the slide, and the value of a focus measure; the latter evaluates the local image sharpness and is generally based on the illumination gradient of an image (He *et al*., 2003; Malik & Choi, 2008). An ideal focus algorithm is regarded as having a maximum value for the focus measure at the best-focused image (Sun *et al.*, 2004; Huang & Jing, 2007). The focus measure increases as the image sharpness increases, attaining a maximum for the sharpest image in a stack. The focal position (the level of the microscope stage) can be estimated from a focus curve, obtained by evaluating each image in a stack to obtain a focus measure and plotting it against focal position. The best focal position is then found by searching for the optimum of the focus curve.

The following criteria are considered in the selection and evaluation of a typical focus measure (Sun *et al.*, 2004; Huang & Jing, 2007; Liu *et al.*, 2007):

1. the focus measure must be unimodal, that is having only one maximum;
2. the system must be in focus at the maximum;
3. the range which describes the distance between two neighbouring local minima around the global maximum over which an in-focus image can be attained must be as large as possible;
4. the focus measure must not be limited to some special types of images;
5. the focus measure must be robust to noise;
6. the focus measure must be computationally fast.

Spatial or frequency domain focus measures may be used (Huang & Jing, 2007); classification of focus measures is discussed by different authors (Santos *et al.*, 1997; Sun *et al.*, 2004; Liu *et al.* 2007). Frequency domain measures are more complex (Krotkov, 1987; Yeo *et al.*, 1993); hence, as a first step towards autofocusing for TB microscopy, we evaluate spatial domain focus measures. Low cost and ease of maintenance have made bright-field microscopy of ZN-stained sputum smears the method of choice for TB screening in developing countries. We examine autofocusing for stacks of images acquired using a bright-field microscope.

Materials and methods

Image acquisition

A bright-field microscope, Nikon eclipse 55i, equipped with a 40×/0.65 numerical aperture objective lens (Nikon Plan) and a custom-made stage was used for imaging the ZN-stained slides. Stage movement in the *x*-and *y*-axes is controlled using Zaber T-LA28 linear actuators and the focus control uses a stepper motor from Tofra. The focus level is controlled through software adjustment of the z-positions of the stage. Images were captured with a Lumenera, Infinity 2-1C 1.4 mega-pixel digital camera and stored with 1392 × 1040-pixel resolution in 8-bit JPEG format. This camera uses a Sony ICX205 sensor with a pixel size of 4.65 μm.

A software script enables images to be captured and stored at fixed intervals along the *z*-axis to produce a single stack of 20 images for a given field of a slide. Varying the position of the stage changes the image sharpness and hence the degree of focus. Each image in a stack, therefore, is at a different focus level. A stack of images for each field was captured by bringing a view field into focus and capturing a set of images along the *z*-axis with the in-focus image at its centre. Stacks were captured from five adjacent fields in each of 13 slides, to give a total of 65 stacks. Manual focusing allowed us to capture stacks symmetrically around the position of optimal focus and produced our in-focus ground truth.

A step size smaller than 1 μm has been suggested to achieve fine focus (Santos *et al.*, 1997), but the smaller the step size, the more images need to be acquired for a stack and hence the longer the image acquisition time. Various formulae have been derived to describe the relationship between the depth of field and the numerical aperture of a microscope objective. We use the relationship suggested by the manufacturers of our microscope (Nikon, 2009)

$$\mathrm{DOF}=\frac{\lambda\eta}{\mathrm{NA}^2}+\frac{\eta e}{M\,(\mathrm{NA})},$$

where λ is the wavelength used (λ = 500 nm mean wavelength in the visible band 300–700 nm), η is the refractive index of the medium (η = 1), NA is the numerical aperture of the objective (NA = 0.65), *M* is the magnification (*M* = 40), *e* is the smallest distance that can be resolved by a detector placed at the image plane and DOF is the depth of field.

The spatial distance that can be resolved by the sensor in our camera has to be at least twice the pixel size of the camera (*P* = 4.65 μm), taking the magnification into account, to satisfy the Nyquist sampling criterion (Geusebroek *et al.*, 2000)

$$2P=M\times e.$$

Thus, *e* = 0.2325 μm and the theoretical depth of field is calculated to be 1.19 μm. We therefore used a step size of 1.2 μm to acquire image stacks.

Focus measures

Due to variations in sputum smears (thickness, staining quality, density of bacilli, presence of debris) and the resulting images, threshold-dependant focus measures were not considered in this study, as a global threshold applicable to all images is unlikely to be obtained. Focus functions optimized for one imaging modality may not perform well with another (Groen *et al.*, 1985) and no generally applicable autofocusing solution has been proposed for microscopy (Geusebroek *et al.*, 2000). Six focus measures, reported to be suitable for a variety of biological and biomedical applications (Santos *et al.*, 1997; Xie *et al.*, 2007; Yazdanfar *et al.*, 2008) were

investigated; the normalized variance, the Brenner gradient, the sum-modified Laplacian, the energy of the Laplacian of the image, Vollath's F_4 and Tenengrad's algorithm.

Normalized variance (Groen *et al.*, 1985; Yeo *et al.*, 1993): this algorithm computes variations in intensity levels among pixels in an image and then compensates for the differences in average image intensity among different images by normalizing the final output with the mean intensity μ

$$F_{\mathrm{NV}} = \frac{1}{M \times N \times \mu} \sum_{i=1}^{M} \sum_{j=1}^{N} [I(i, j) - \mu]^2,$$

where I is the pixel intensity at (i,j), M and N are the height and width of the image, respectively.

Brenner gradient, originally suggested by Brenner *et al.* (1976), is a fast edge detector, which measures the difference between a pixel and a neighbour (Yazdanfar *et al.*, 2008).

$$F_{\mathrm{Brenner}} = \sum_{i=1}^{M} \sum_{j=1}^{N} [I(i, j) - I(i+m, j)]^2,$$

where $m = 2$, that is a neighbour is two pixels away.

Sum-modified-Laplacian (SML) (Nayar & Nakagawa, 1994): this focus measure calculates the sum of the absolute values of the convolution of an image with modified Laplacian operators. The modified Laplacian takes the absolute values of the second derivatives in the Laplacian to avoid the cancellation of second derivatives in the horizontal and vertical directions that have opposite signs

$$\nabla_M^2 I = \left| \frac{\partial^2 I}{\partial i^2} \right| + \left| \frac{\partial^2 I}{\partial j^2} \right|,$$

where I is the image intensity at point (i, j).

The discrete approximation to the Laplacian is normally a 3 × 3 operator and to accommodate possible variations in the size of texture elements, the partial derivatives are computed using a variable spacing (*step*) between the pixels used to compute the derivatives; we use *step* = 1 in our implementation. The discrete approximation of the modified Laplacian is therefore given by

$$\begin{aligned} \nabla_M^2 (i, j) = \; & |2I(i, j) - I(i - step, j) - I(i + step, j)| \\ & + |2I(i, j) - I(i, j - step) - I(i, j + step)| . \end{aligned}$$

The focus measure at a point (x,y) is computed as the sum of the modified Laplacian, in a window around the point

$$F_{\mathrm{SML}}^{(x,y)} = \sum_{i=x-N}^{x+N} \sum_{j=y-N}^{y+N} \nabla_M^2 (i, j),$$

where the N is a parameter that determines the window size used to compute the focus measure.

Energy of Laplacian of the image (EOL) (Huang & Jing, 2007): this focus measure analyses high spatial frequencies associated with image border sharpness using the Laplacian operator:

$$F_{\mathrm{EOL}} = \sum_{i}^{M} \sum_{j}^{N} \left(I_{ii} + I_{jj} \right)^2,$$

where I_{ii} and I_{jj} are second derivatives of I with respect to i and j, respectively, and their summation is given by

$$\begin{aligned} I_{ii}+I_{ij} = \; & -I(i-1, j-1) - 4 \times I(i-1, j) \\ & -I(i-1, j+1) - 4 \times I(i, j-1) \\ & +20 \times I(i, j) - 4 \times I(i, j+1) - I(i+1, j-1) \\ & -4 \times I(i+1, j) - I(i+1, j+1). \end{aligned}$$

Vollath's F_4 (Vollath, 1988) is based on the autocorrelation function and was reported to provide good performance in the presence of noise

$$\begin{aligned} F_{\mathrm{Vollath}} = \; & \sum_{i=1}^{M-1} \sum_{j=1}^{N} I(i, j) \times I(i+1, j) \\ & - \sum_{i=1}^{M-2} \sum_{j=1}^{N} I(i, j) \times I(i+2, j). \end{aligned}$$

Tenenbaum's algorithm (Tenengrad) (Yeo *et al.*, 1993) is a gradient magnitude maximization method that measures the sum of the squared responses of the horizontal and vertical Sobel masks.

$$F_{\mathrm{Tenengrad}} = \sum_{i=2}^{M-1} \sum_{j=2}^{N-1} (\nabla I(i, j))^2,$$

where $\nabla I(i, j)$ is the Sobel gradient magnitude value (Gonzalez & Woods, 2001) given by:

$$\nabla I(i, j) = \sqrt{\nabla I_i(i, j)^2 + \nabla I_j(i, j)^2}.$$

In its original implementation, the summation is for pixels that are above a certain threshold, however, we chose to use a variation in which all pixel locations can be included in the summation (Santos *et al.*, 1997). The Tenengrad function was reported to perform adequately with bright-field microscopy images, although it may produce local maxima (Valdecasas *et al.*, 2001).

Each focus measure was computed for all the images of a particular stack and the value of the focus measure was plotted against distance from the starting point. Images were captured at fixed positions for each stack. Several published methods have selected the position of the image with the highest focus measure value as the optimal focus position (Groen *et al.*, 1985; Subbarao & Tyan, 1998; Valdecasas *et al.*, 2001; Sun *et al.*, 2004; Yazdanfar *et al.*, 2008). This assumes that the focus position occurs at one of the steps; however, the optimal

focus position may lie between the fixed image positions. Therefore, a fast Fourier transform-based interpolation method was used to interpolate the focus function between the fixed steps so that the values of the function between these steps could be estimated. The curves were analysed to determine the distance between the global maximum and the best focused image (located manually).

Optimizing the focus search

A number of search methods have been proposed for finding the position of optimal focus, to reduce lens motion and achieve faster autofocus times. The simplest search method scans all possible lens positions and computes the associated focus function. The algorithm then moves the lens back to the position where the highest value for the focus measure was obtained.

The difference of signs method (Svahn, 1996) computes the focus measure at an initial lens position and then moves to the next position where the focus measure is computed again; the difference in the focus measure values is obtained and if the difference is positive, the lens movement is continued in this direction, otherwise the direction is reversed and the lens is moved in small steps until a peak value is reached.

Another method combines the difference of signs technique, a Fibonacci or binary search and interpolation, to minimise lens motion (Subbarao & Tyan, 1998). In this method, the difference of signs determines the correct direction in which to move the lens and a sequential search is then carried out in this direction by moving the lens in small steps until the first decrement in the focus measure is detected. A Fibonacci or binary search is carried out in the interval containing the final three lens positions in order to narrow the interval, and then a Gaussian or quadratic function is fitted to three or more points in this interval to locate the position of maximum focus.

The above-mentioned search methods pass the optimal focus position multiple times, with extensive and time-consuming mechanical motion (Svahn, 1996). Yazdanfar *et al.* (2008) proposed an approach that reduces the number of intermediate images evaluated: a curve may be fitted to the focus measures of a few images selected at different positions along the *z*-axis, the peak of the curve representing the focal position. Focus function curves are generally Gaussian in shape near their peak values (Nayar & Nakagawa, 1994). Fitting a Gaussian function requires an estimate of the standard deviation of the data as an intermediate stage; it is difficult to find an accurate value for the standard deviation using few sampling points. However, fitting a Gaussian function to a data set is equivalent to fitting a quadratic function to its logarithm (Smith, 2008). To fit a polynomial of order n,atleast $n + 1$ images have to be acquired; therefore, three images are needed to find the position of optimal focus.

An implementation of automated TB microscopy would require a number of fields to be examined in any slide. Our proposed autofocusing method follows the curve-fitting approach of Yazdanfar *et al.* (2008) for fields other than the first one to be evaluated in a slide. A full image stack is captured and a global search for the focal position performed only for the first field in each slide, ensuring a comprehensive evaluation of this field to avoid locating the position of optimal focus at a local minimum and propagating the associated error through the slide. The curve-fitting approach in subsequent fields minimizes the number of images to be evaluated.

For fields other than the first on the slide, images for curve fitting are located on either side of the focal position found in the previous field. The positioning of the images relative to the position of optimal focus influences the quality of the fit and therefore the accuracy of focal point estimation. The prediction accuracy decreases as the distance from the focal position at which images are captured for fitting increases. For this reason, one image is captured at a

distance equal to a stepsize from the focal position of the previous field (as determined manually) and the second and third images are captured at distances of one and two stepsizes, respectively, on the other side. Thus, the lens movement is kept to a minimum, reducing the focusing time. Processing was done in Matlab.

Performance evaluation

The performance of the focus functions was evaluated in two stages; first, a qualitative analysis was carried out by visual inspection. Then, to rank the performance of the focus measures, a quantitative analysis was carried out. For the quantitative analysis, we added the execution time to the criteria employed by Firestone *et al.* (1991), namely accuracy, range, full width at half maximum and number of false maxima. The time taken for mechanical motion of the stage was not taken into account. The features used in evaluation are defined as follows:

1. *Execution time*: the time taken for an algorithm to compute the focus plot and locate the position of maximum focus.
2. *Range*: the interval where the focus plot exhibits monotonic decrement from the maximum.
3. *Accuracy*: the difference (μm) between the position of the peak of the focus plot and the position of focus as determined by an expert.
4. *Full width at 50% of the peak (FWHM)*: the interval between the positions at which the value of the focus measure is half of the maximum.
5. *Number of false maxima*: local peaks in the focus plot which do not correspond to the in-focus image.

A quantitative evaluation may compare a focus curve to an ideal function with respect to each of these characteristics (Santos *et al.*, 1997; Sun *et al.*, 2004). An ideal focus function was defined as having a value of0for execution time, accuracy, FWHM and number of false maxima and a range of 22.8 μm, determined by the number of images in the stack (20) and the step size (1.2 μm); in an ideal situation, the in-focus image is located at the centre of the stack and the focus function is expected to decrease monotonically from the peak throughout the entire length of the stack. For each focus measure, the absolute difference between the value of each feature and its corresponding ideal value was computed; a rank from 1 (the focus measure deviating least from the ideal function) to 5 (the focus measure deviating most from the ideal function) was assigned. A global ranking score was then obtained for each function by adding all the individual feature scores, the function with the lowest global score being the best performing method.

Focus measures were compared for full stacks and for curves fitted to subsets of images around the focal position.

Results

For each stack, focus measures were computed for each image and plotted against distance. Figure 1 shows the focus measure plot obtained for normalized variance. Figure 2 shows the typical plots obtained for the sum-modified Laplacian, energy of the image Laplacian, Vollath's F_4, Brenner gradient and Tenengrad for both original (obtained from the stack of 20 images) and fitted curves (fitted using three images); the values of the focus measures have been normalized by their respective maximum values to allow for comparison.

In Fig. 2, the position of maximum focus is indicated on each plot by the vertical dashed line whereas the circles indicate the positions at which the images used for curve-fitting were

captured, around the focal position of the previous adjacent stack. Figure 3 shows examples of in-focus images from different slides.

Table 1 shows the average feature values for each focus function for the original curves and the corresponding rank of each focus measure. The performance evaluation was carried out offline and therefore the execution times do not include the time for z-motor movement. The global score, obtained by adding the individual feature scores, as well as the overall ranking of the focus functions, are included in the table. Only accuracy and processing time are considered in the assessment of curve fitting performance, given in Table 2.

The average difference in manually determined focal positions of adjacent fields was 1.26 μm, with the highest of 4 μm found for poorly prepared slides.

Discussion

Five of the six focus measures studied, namely SML, EOL, Brenner gradient, Vollath's F_4 and Tenengrad have the expected Gaussian-shaped plots. Focus curves for normalized variance do not display the expected Gaussian shape, hence no further analysis was carried out using this focus measure.

The performance of the normalized variance is different from what has been reported in other studies. Sun *et al.* (2004) ranked normalized variance the best overall focus function for bright-field imaging of several types of tissue and it was ranked second in a study by Firestone *et al.* (1991) for imaging tissue sections; a similar result was recorded by Yazdanfar *et al.* (2008) for bright-field imaging of histopathology tissue sections, with no false maxima. The large range of the z-stack may result in the images at its extremes containing features not present at the focal position and causing large image variance, regardless of a lack of image sharpness. Figure 1 shows the normalized variance having a local peak around the centre of the stack and the position of optimal focus.

SML and EOL perform similarly with respect to all features except for processing time, and produce similar curve shapes, which differ only in their magnitude. The Brenner gradient has the shortest processing times but ranks below Tenengrad and Vollath's F_4 with respect to accuracy, range and FWHM and has the lowest rank with respect to local maxima. In the study of Sun *et al.* (2004), the Brenner gradient was ranked fifth, ahead of SML and EOL but below Tenengrad and higher than Vollath's F_4. Tenengrad performs well, achieving the highest rank with respect to the range, accuracy and FWHM criteria. This result agrees well with other published studies (Santos *et al.* 1997; Pech-Pacheco *et al.*, 2000; Huang & Jing, 2007), particularly that of Sun *et al.* (2004), in which it had the third best accuracy and was second only to Vollath's F_4 in terms of FWHM under bright-field imaging. However, the long processing times impact negatively on its overall ranking; a drawback noted in other studies (Santos *et al.*, 1997; Huang & Jing, 2007). Vollath's F_4 shows consistent performance with regard to all the features; its curves have a sharp and distinct peak with few local maxima. Vollath's F_4 was also the best overall focus measure in the study by Santos *et al.* (1997).

Results for curve fitting follow a similar trend to that observed in the plots for full stacks, except for the Brenner gradient ranking first along with Vollath's F_4. Average accuracies displayed in Tables 1 and 2 are less than the step size, that is within the depth of field of the microscope. The average difference in manually determined focal positions of adjacent fields was close to the step size, in spite of relatively large differences (up to 4 μm) for poorly prepared slides. Therefore, the approach of using the focal position from a previous field as an estimate for the subsequent field is viable for well prepared slides. Samples on poorly prepared slides are thick and objects are present at different depths, producing multiple focal planes in one field. Local maxima observed in some plots (Fig. 2d) may be attributed to multiple focal planes.

For the computation of the focus measures, images are converted from RGB to grey scale. Because we are interested in detecting the presence of red bacilli, exploring the application of focus measures to different colour channels in different colour spaces may reveal combinations that preferentially seek images in which bacilli are maximally in focus, especially in poorly prepared smears.

We have used manually rather than automatically located focal positions as a basis for curve fitting for subsequent fields because evaluation was done offline; however, the accuracies of automatically located focal positions were much lower than a step size, indicating that similar curve fitting results may be expected when using automatically located focal position estimates. In a practical implementation of autofocusing across an entire slide, manual selection of the z-window within which a stack is acquired for the first field would be undesirable, and a larger stack may have to be acquired of the first field to ensure adequate coverage.

In practical autofocusing applications, the time taken for the mechanical motion of the objective with respect to the stage is the greatest source of delay (Subbarao & Tyan, 1998). Thus, the execution times shown in Tables 1 and 2 do not reflect those of a full autofocusing implementation. The processing times recorded in this study may be improved by using a faster programming language such as C++ in a parallel processing environment.

We have tested the suitability of various autofocusing methods for automated microscopy, as a step towards an automated slide analysis system and have isolated the software processing components of autofocusing for evaluation. Integration of autofocusing with slide movement is a future target towards automation.

Conclusion

We have presented a comparison of existing autofocus measures for digital microscopy and applied them to bright-field imaging of ZN-stained sputum smear slides, with the aim of determining which method performs best for automated microscopy to detect TB. Vollath's F_4 gave the best overall performance on full stacks but both Brenner gradient and Vollath's F_4 ranked the best under curve fitting. The focal position of a field may be used as an estimate of that of an adjacent field, to reduce focusing time.

Acknowledgments

This work was supported by the NIH/NIAID under Grant 5R21AI067659-02.

References

Brenner JF, Dew BS, Horton JB, King T, Neurath PW, Selles WD. Automated microscope for cytologic research - preliminary evaluation. J. Histochem. Cytochem 1976;24:100–111. [PubMed: 1254907]

Firestone L, Cook K, Culp K, Talsania N, Preston K. Comparison of autofocus methods for automated microscopy. Cytometry 1991;12:195–206. [PubMed: 2036914]

Forero MG, Sroubek F, Cristobal G. Identification of tuberculosis bacteria based on shape and color. Real-Time Imaging 2004;10:251–262.

Forero MG, Cristobal G, Desco M. Automatic identification of Mycobacterium tuberculosis by Gaussian mixture models. J. Microsc.-Oxford 2006;223:120–132.

Geusebroek J, Cornelissen F, Smeulders AWM, Geerts G. Robust autofocusing in microscopy. Cytometry 2000;39:1–9. [PubMed: 10655557]

Gonzalez, RC.; Woods, RE. Digital Image Processing. Prentice Hall; New Jersey: 2001.

Groen FCA, Young IT, Ligthart G. A comparison of different focus functions for use in autofocus algorithms. Cytometry 1985;6:81–91. [PubMed: 3979220]

He J, Zhou RZ, Hong ZL. Modified fast climbing search auto-focus algorithm with adaptive step size searching technique for digital camera. IEEE Transact. Consum. Electron 2003;49:257–262.

Huang W, Jing Z. Evaluation of focus measures in multi-focus image fusion. Pattern Recogn. Lett 2007;28:493–500.

Khutlang R, Krishnan S, Whitelaw A, Douglas TS. Automated detection of tuberculosis in Ziehl-Neelsen stained sputum smears using two one-class classifiers. J. Microsc.-Oxford 2010;237:96–102.

Khutlang R, Krishnan S, Dendere R, Whitelaw A, Veropoulos K, Learmonth G, Douglas TS. Classification of *Mycobacterium tuberculosis* in images of Z.N.-stained sputum smears. IEEE Transact. Informat. Technol. Biomed. in press. DOI 10.1109/TITB.2009.2028339.

Krotkov E. Focusing. Int. J. Comput. Vis 1987;1:223–237.

Liu XY, Wang WH, Sun Y. Dynamic evaluation of autofocusing for automated microscopic analysis of blood smear and pap smear. J. Microsc.-Oxford 2007;227:15–23.

Malik AS, Choi TS. A novel algorithm for estimation of depth map using image focus for 3D shape recovery in the presence of noise. Pattern Recogn 2008;41:2200–2225.

Nayar SK, Nakagawa Y. Shape from Focus. IEEE Transact. Pattern Anal. Mach. Intell 1994;16:824–831.

Nikon MicroscopyU: Articles - Formulas. [last accessed 14 December 2009]. http://www.microscopyu.com/articles/formulas/formulasfielddepth.html

Pech-Pacheco, JL.; Cristobal, G.; Chamorro-Martinez, J.; Fernandez-Valdivia, J. Diatom autofocusing in brighfield microscopy: a comparative study. 15th International Conference on Pattern Recognition; Barcelona. 2000. p. 3

Sadaphal P, Rao J, Comstock GW, Beg MF. Image processing techniques for identifying Mycobacterium tuberculosis in Ziehl-Neelsen stains. Int. J. Tuberc. Lung Dis 2008;12:579–582. [PubMed: 18419897]

Santos A, De Solorzano CO, Vaquero JJ, Pena JM, Malpica N, Del Pozo F. Evaluation of autofocus functions in molecular cytogenetic analysis. J. Microsc.-Oxford 1997;188:264–272.

Smith, JO. Spectral Audio Signal Processing. 2008. http://ccrma. stanford.edu/j̃os/sasp/, online book, last accessed 5 July 2009

Steingart K, Henry M, Ng V, et al. Fluorescence versus conventional sputum smear microscopy for tuberculosis: a systematic review. Lancet Infect. Dis 2006;6:570–581. [PubMed: 16931408]

Subbarao M, Tyan JK. Selecting the optimal focus measure for autofocusing and depth-from-focus. IEEE Transact. Pattern Anal. Mach. Intell 1998;20:864–870.

Sun Y, Duthaler S, Nelson BJ. Autofocusing in computer microscopy: selecting the optimal focus algorithm. Microsc. Res. Tech 2004;65:139–149. [PubMed: 15605419]

Svahn, F. MSc Thesis. Tekniska Hogskolan Linkoping; 1996. Tools and methods to obtain a passive autofocus system.

Valdecasas AG, Marshall D, Becerra JM, Terrero JJ. On the extended depth of focus algorithms for bright field microscopy. Micron 2001;32:559–569. [PubMed: 11166576]

Veropoulos K, Learmonth G, Campbell C, Knight B, Simpson J. Automated identification of tubercle bacilli in sputum - A preliminary investigation. Anal. Quant. Cytol. Histol 1999;21:277–282. [PubMed: 10560504]

Vollath D. The influence of the scene parameters and of noise on the behavior of automatic focusing algorithms. J. Micros.-Oxford 1988;151:133–146.

Xie H, Rong WB, Sun LN. Construction and evaluation of a wavelet-based focus measure for Microscopy Imaging. Microsc. Res. Tech 2007;70:987–995. [PubMed: 17661388]

Yazdanfar S, Kenny KB, Tasimi K, Corwin AD, Dixon EL, Filkins RJ. Simple and robust image-based autofocusing for digital microscopy. Opt. Express 2008;16:8670–8677. [PubMed: 18545580]

Yeo TTE, Ong SH, Jayasooriah Sinniah, R. Autofocusing for tissue microscopy. Image Vis. Comput 1993;11:629–639.

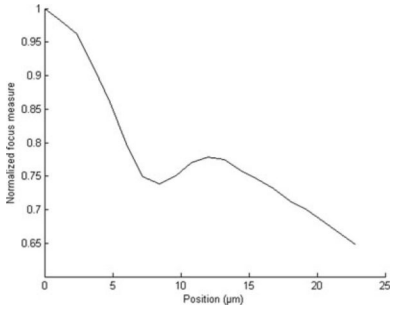

Fig. 1.
Typical focus measure plot for normalized variance.

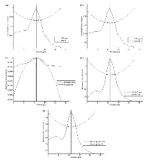

Fig. 2.

Typical focus measure functions extracted from the full stack of 20 images (solid curve) and fitted to only three images (dashed curve): (a) sum-modified Laplacian, (b) energy of image Laplacian, (c) Tenengrad, (d) Vollath's F4 and (e) Brenner gradient. The circles represent the position at which the three images used for fitting were captured. The vertical dashed line represents the position of the maximum of the 20 z-stack values while the vertical solid line represents the minimum (or maximum) of the fitted curves; the difference in orientation of the three-image fitted curves is due to the difference in sign of the logarithms of corresponding focus function values.

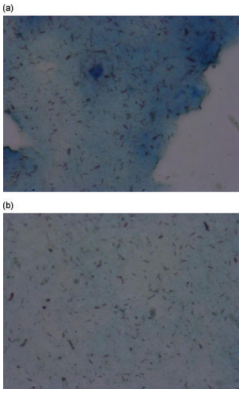

Fig. 3.
Example in-focus images from different stacks.

Table 1

Comparison of the deviation of the focus functions from the ideal function, using a full stack.

	SML		EOL		Tenengrad		Vollath's F_4		Brenner gradient	
	Mean (SD)	**Rank**	**Mean (SD)**	**Rank**	**Mean (SD)**	**Rank**	**Mean (SD)**	**Rank**	**Mean (SD)**	**Rank**
Accuracy (μm)	0.36 (0.17)	4	0.36 (0.20)	4	0.27 (0.15)	1	0.27 (0.11)	1	0.30 (0.15)	3
Time (s)	5.77 (0.04)	3	7.24 (0.03)	4	14.86 (0.04)	5	5.27 (0.10)	2	4.69 (0.02)	1
Range (μm)	10.8 (1.70)	5	9.90 (1.15)	4	4.30 (3.10)	1	6.60 (1.35)	2	8.13 (2.46)	3
FWHM (μm)	5.58 (0.81)	5	5.37 (0.82)	4	4.80 (0.42)	1	4.95 (0.55)	2	4.98 (0.79)	3
False maxima	2 (0.82)	3	2 (0.82)	3	0.75 (1.50)	2	0.25 (0.50)	1	1.00 (0)	5
Global score		20		19		10		8		15
Global rank		5		4		2		1		3

Table 2

Comparison of focus functions under curve fitting.

	SML		EOL		Tenengrad		Vollath's F_4		Brenner gradient	
	Mean (SD)	**Rank**	**Mean (SD)**	**Rank**	**Mean (SD)**	**Rank**	**Mean (SD)**	**Rank**	**Mean (SD)**	**Rank**
Accuracy (μm)	0.30 (0.23)	4	0.30 (0.23)	4	0.27 (0.15)	3	0.15 (0.23)	1	0.18 (0.07)	2
Time (s)	0.93 (0.01)	3	1.15 (0.01)	4	2.30 (0.01)	5	0.86 (0.01)	2	0.73 (0.01)	1
Global score	7		8		8		3		3	
Global rank	3		4		4		1		1	